PROCEEDINGS OF SPIE

SPIEDigitalLibrary.org/conference-proceedings-of-spie

A spherical mirror-based illumination system for fluorescence excitation-scanning hyperspectral imaging

Samantha Gunn Mayes, Samuel A. Mayes, Craig Browning, Marina Parker, Thomas C. Rich, et al.

Samantha Gunn Mayes, Samuel A. Mayes, Craig Browning, Marina Parker, Thomas C. Rich, Silas J. Leavesley, "A spherical mirror-based illumination system for fluorescence excitation-scanning hyperspectral imaging," Proc. SPIE 10881, Imaging, Manipulation, and Analysis of Biomolecules, Cells, and Tissues XVII, 108810N (4 March 2019); doi: 10.1117/12.2510553



Event: SPIE BiOS, 2019, San Francisco, California, United States

A Spherical Mirror-based Illumination System for Fluorescence Excitation-Scanning Hyperspectral Imaging

Samantha Gunn Mayes¹, Samuel A. Mayes^{1,4}, Craig Browning^{1,4}, Marina Parker^{1,4}, Thomas C. Rich ^{2,3}, Silas J. Leavesley^{1,2,3}

¹Department of Chemical and Biomolecular Engineering, ²Department of Pharmacology, ³Center for Lung Biology, University of South Alabama, ⁴Department of Systems Engineering

ABSTRACT

Many hardware approaches have been developed for implementing hyperspectral imaging on fluorescence microscope systems; each with tradeoffs in spectral sensitivity and spectral, spatial, and temporal sampling. For example, tunable filter-based systems typically have limited wavelength switching speeds and sensitivities that preclude high-speed spectral imaging. Here, we present a novel approach combining multiple illumination wavelengths using solid state LEDs in a 2-mirror configuration similar to a Cassegrain reflector assembly. This approach provides spectral discrimination by scanning a range of fluorescence excitation wavelengths, which we have previously shown can improve spectral image acquisition time compared to traditional fluorescence emission-scanning hyperspectral imaging. In this work, the geometry of the LED and other optical components was optimized. A model of the spectral illuminator was designed using TracePro ray tracing software (Lambda Research Corp.) that included an emitter, lens, Spherical mirror, flat mirror, and liquid light guide input. A parametric sensitivity study was performed to optimize the optical throughput varying the LED viewing angle, properties of the Spherical reflectors, the lens configuration, focal length, and position. The following factors significantly affected the optical throughput: LED viewing angle, lens position, and lens focal length. Several types of configurations were evaluated, and an optimized lens and LED position were determined. Initial optimization results indicate that a 10% optical transmission can be achieved for either a 16 or 32 wavelength system. Future work will include continuing to optimize the ray trace model, prototyping, and experimental testing of the optimized configuration.

Keywords: Spectral, Spectroscopy, Fluorescence, Microscope, Microscopy, Imaging, Bioimaging, HSI

1.0 INTRODUCTION

Traditional fluorescence imaging uses exogenous dyes or proteins to visualize molecular structures and activity. Fluorescent labels each have respective excitation and emission peak wavelengths and spectral signatures. ¹² Detection at these peak wavelengths enables preferential imaging of one or more of the fluorescence labels. Hyperspectral imaging (HSI) expands on this concept by collecting contiguous spectral data at each pixel. ^{3–6} Normally, HSI systems separate the emitted fluorescence into different spectral bands using one of many approaches for spectral filtering or dispersion. ^{3,7–9} However, these systems often introduce some loss of signal in the spectral filtering or dispersion process.

Traditional fluorescence-microscope based hyperspectral imaging methods often necessitate tradeoffs in spectral sensitivity and spectral, spatial, and temporal sampling. We are currently working to develop spectral fluorescence excitation systems that overcome some of these tradeoffs by using a pair of beam-combining mirrors and multiple illumination wavelengths to acquire images at faster speeds while maintaining a high signal to noise ratio. We have developed an excitation-scanning hyperspectral imaging technology that provides a range of spectral illumination wavelengths with narrow band resolution. As the sample is excited at each band of illumination, the entire emission spectra can be detected. The composite image across the entire excitation spectrum provides hyperspectral discrimination. ^{10–12} However, further work is needed to improve temporal, spatial, and spectral sampling by optimizing the illumination delivery to the sample in this excitation scanning setup.

Here, we present results from an initial software model that was developed to optimize the optical transmission of excitation illumination. The optical geometry was optimized using Monte Carlo optical ray trace modeling. This

Imaging, Manipulation, and Analysis of Biomolecules, Cells, and Tissues XVII, edited by Daniel L. Farkas, Attila Tarnok, James F. Leary, Proc. of SPIE Vol. 10881, 108810N · © 2019 SPIE · CCC code: 1605-7422/19/\$18 · doi: 10.1117/12.2510553

information can be used to optimize the optical pathway of the light source with end-user applications in endoscopy and microscopy . 13–16

2.0 METHODS

2.1 Optical Configuration Setup

TracePro software (Lambda Research Corporation) was used to simulate the Spherical mirror array which included a flat mirror, a larger concave Spherical mirror, LEDs, and up to two different lenses as shown in Figure 1. The figure displays the curved mirror at the top with a small round surface at its center that represents the liquid light guide input (LLGI). A smaller flat mirror was positioned directly underneath the curved mirror. The LED was represented by a small cube located at the bottom of the model. Above the LED, either 1 or 2 lenses were located. Two different lens configurations were evaluated: a configuration with one focusing lens (Figure 1, left) and a configuration with a collimating and a focusing lens (Figure 1, right). TracePro allowed importing different off-the-shelf lenses with different focal lengths (FL) from data files on the manufacturer website.

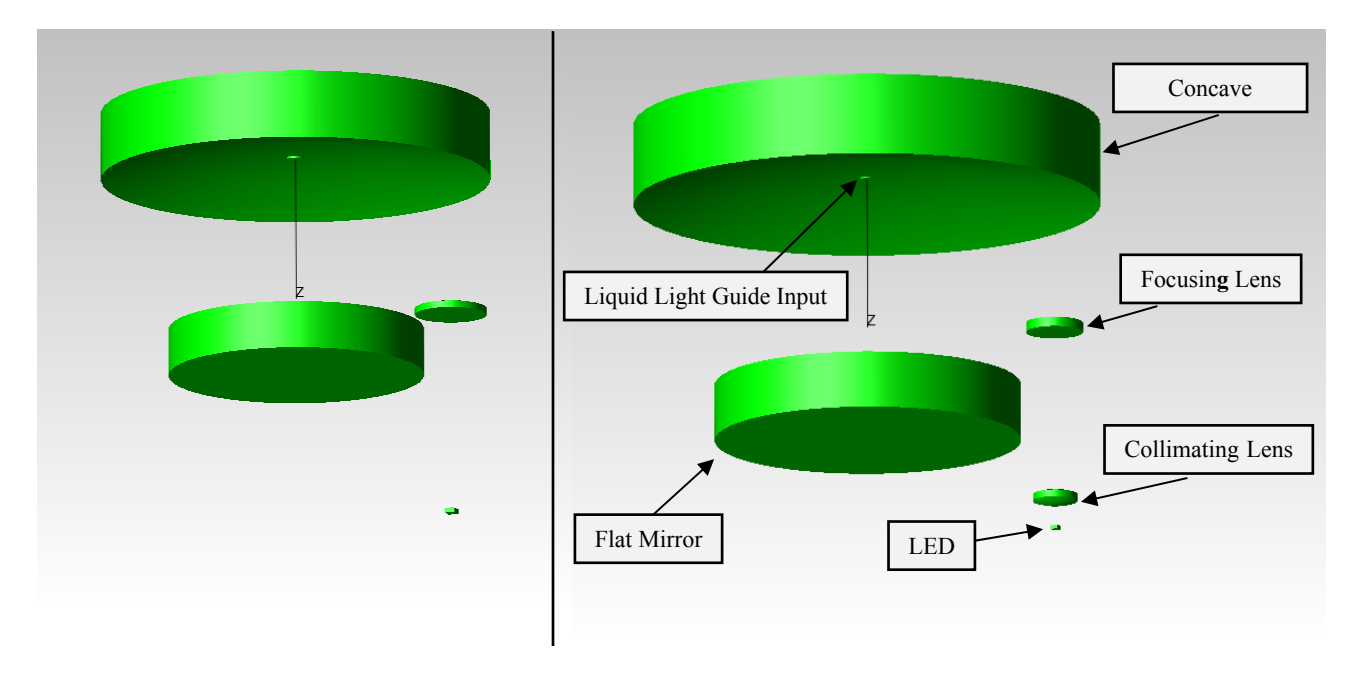


Figure 1 - A screenshot of the optical ray trace model in Tracepro showing the single lens configuration (left) and a dual lens configuration (right). The single-lens configuration was used for refocusing the emitted light at a distance corresponding to the entrance of the liquid light guide. The dual-lens configuration was used to collimate and then refocus the emitted light at the liquid light guide entrance aperture.

LED properties were generated in TracePro by importing data from manufacturer's specification sheets. For this model, a 525 nm LED with high power output and low dispersion angle was used (part # SMB1N-525V-02, Roithner LaserTechnik GmbH). The generated surface source property was then assigned to the top surface of the object representing the LED for simulating ray traces similar to the one shown in Figure 2. In this example figure, rays exit the top surface of the LED and are focused by a 100 mm FL lens. Rays were reflected from the edge of the curved mirror to the flat mirror and then to the center of the curved mirror where the LLGI is located. The LLGI surface was defined as a perfect absorber and an irradiance map of incident rays upon the LLGI was generated in order to display the number and distribution of incident rays upon the LLGI.

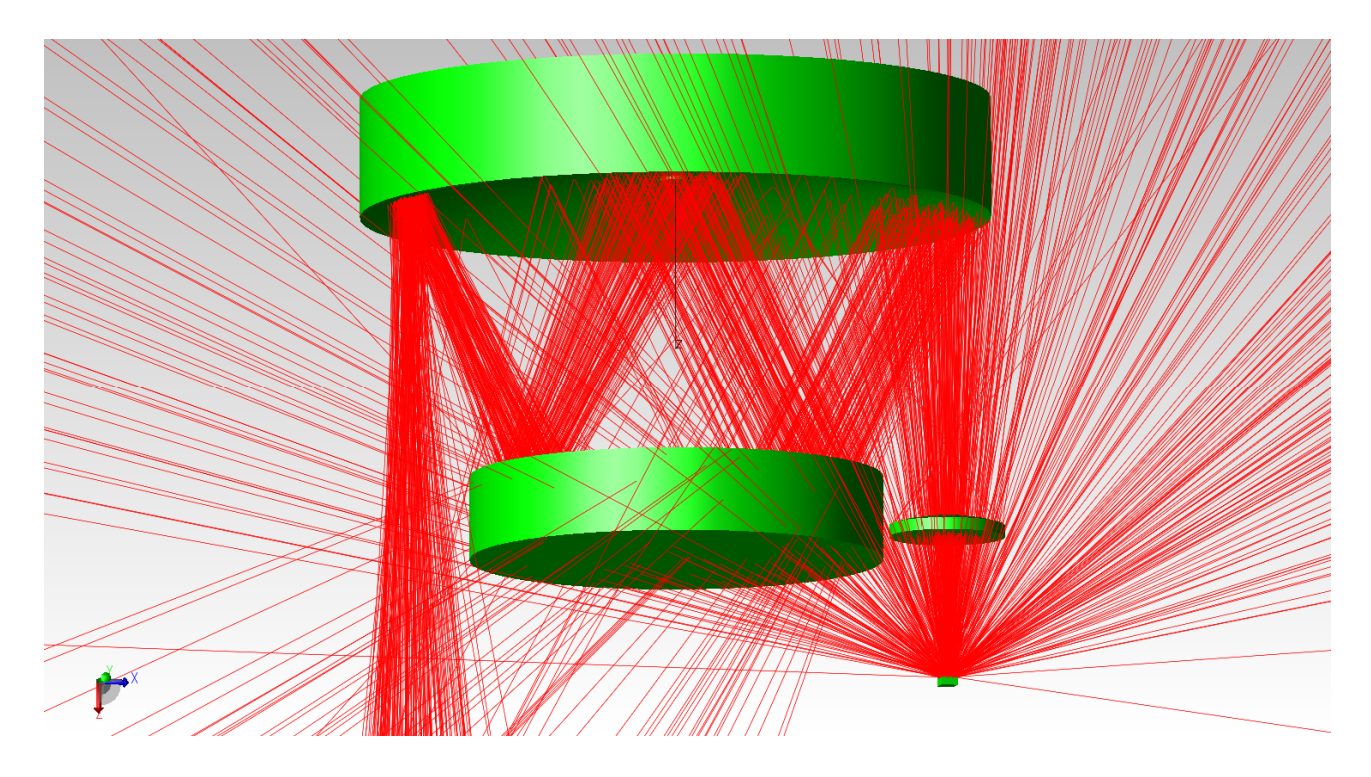


Figure 2 – An image of a single 100 mm FL lens configuration displaying 5 % of the 100,000 rays traced for visualization purposes. Shown in green is the current model featuring the Spherical mirror, flat mirror, LED and lens and shown in red are the rays the ray trace software simulated.

2.2 Parameters Optimized

The optical transmission was optimized through a parametric study using incident rays on the LLGI as the dependent variable and a variety of independent variables, including: lens focal length, lens position, LED position, number of lenses, LED viewing angle, mirror diameter, and mirror curvature. TracePro software provided incident ray results via an irradiance map, an example which is shown in Figure 3. The irradiance map displayed the incident ray distribution on the interrogation surface (LLGI) and the total flux, flux/emitted flux, and the number of incident rays. This information was used to optimize the model by representing the theoretical optical transmission efficiency. A systematic sensitivity study was performed by varying one optical or geometric parameter at a time and measuring the optical transmission efficiency. The first parameter varied was the x and z position of the focusing lens in the single lens configuration (Figure 1, left). Optical transmission data was plotted to visualize the parametric sensitivity response. Four different focal length (FL) lenses were evaluated with this method including a 45 mm, 60 mm, 75 mm, and 100 mm FL. Each of these lenses were evaluated in an optical array using either a 152.4-mm, 114.3-mm, or 76.2-mm FL concave mirror. An additional element was added to each configuration to evaluate the effects of a 12 mm FL collimating lens (Figure 1, right). The 12 mm FL lens was added below each of the focusing lenses and the x and z position were varied along with the focusing lens positions.

After evaluating directional parameters, the viewing angle of the LED was evaluated by dividing the irradiance angular profile of the LED by an integer value, thereby generating a new LED irradiance angular profile. The revised angular illumination profiles were evaluated using the 152.4-mm FL concave mirror with single or dual lens configurations. The dual lens configuration was simulated with 75 mm and 100 mm FL focusing lenses. While optimizing the LED viewing angle, additional perfect absorber objects were added to the configuration at the two points where rays were reflected in the mirror assembly to determine the amount of light lost at each intersection point in the configuration via the irradiance map.

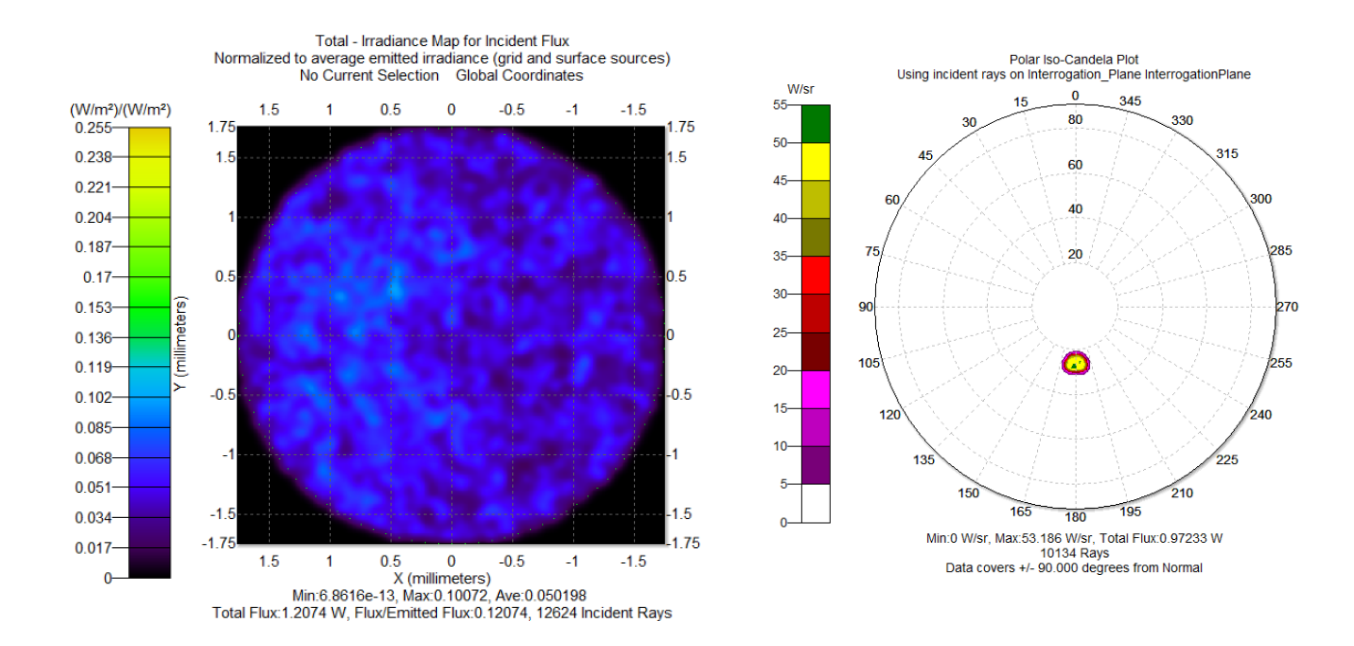


Figure 3 – An example irradiance map generated from the ray trace using a 3.5 mm LLGI (shown left) of the rays incident on the LLGI using a 3inch FL concave mirror and a 45 mm FL single lens configuration and a Polar iso-Candela Plot (shown right) which displays the angular distribution of rays incident on the LLGI.

3.0 RESULTS

Initial results demonstrate that spacing of lenses and LEDs have a large effect on the optical power that can be coupled into the liquid light guide. The data that was taken via the irradiance map was organized and plotted for each configuration to generate a series of parametric sensitivity plots, an example of which can be seen in Figure 4. For each configuration, the data exhibited no increase in transmission after the LED z-position reached a certain distance. Once this distance was reached, transmission remained constant for each lens position that was an equal distance away from the LED. For instance, in Figure 4 after reaching an LED z-position of 70 mm away from the origin, the peak transmission was achieved when the lens was 45 mm away from the LED. This trend continued as the LED was moved further back with each peak remaining where the distance between the lens and LED was 45 mm. This optimization demonstrated the 76.2-mm FL mirror configuration yielded the highest power output with a single 45 mm FL lens.

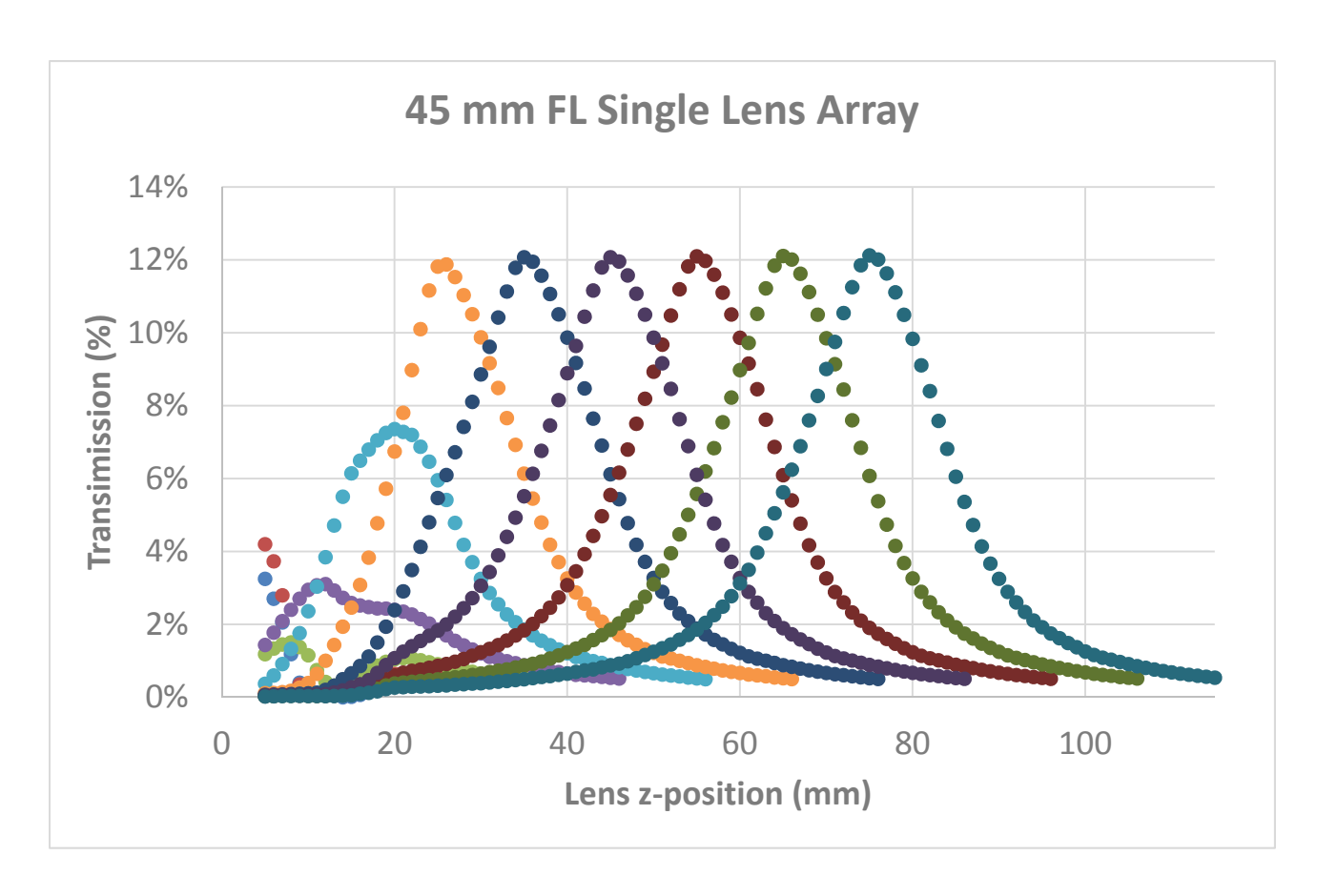


Figure 4 – Graph of transmission vs. lens z-position for each LED z-position evaluated, using a 45 mm FL lens in a 76.2-mm FL concave mirror configuration. The positions used are shown as relative to the origin in the model by distance of millimeters. Each different colored distribution on the graph represents a specific LED z-position, evaluated in increments of 10 mm. For each LED z-position the lens was moved in 1 mm increments starting at the top of the mirror and ending at the LED. Each point on the graph represents the percent transmission at each lens position for a specified LED position.

A sensitivity study of the LED viewing angle using the 525 nm wavelength LED revealed that an approximate 200% increase in optical transmission efficiency could be achieved when the irradiance angular profile was divided by an integer value of 2, providing a similar-shaped angular illumination profile, but with 1/2 the full width at half maximum (FWHM) angle. Results also showed that, for a single lens configuration, the increased power output was linear when the viewing angle was reduced while for a dual lens configuration the power output increase was exponential (Figure 5). To further investigate light losses within the model, irradiance maps were generated for each intersecting surface. This revealed that, for the manufacturer-provided angular irradiance profile, only 20% of the rays intersected the first point at the curved mirror. By comparison, when the FWHM was reduced to less than 10°, more than 50% of the rays emitted intersected the curved mirror. These results indicate using a smaller viewing angle (~10°) would be optimal for design of the system.

The maximum power output achieved through this study was 12% in the 76.2-mm FL mirror configuration. The concave mirror simulated was 3 inches in diameter and could accommodate 12, 15 mm diameter lenses. 12 lenses limited the system to having only 12 LEDs and for additional lenses to be added to the system the diameter and curvature of the 76.2-mm FL mirror were further optimized. Altering the curvature of the mirror reduced the distance needed between the flat mirror and the curved mirror to maintain a similar power output. Enlarging the diameter of the mirror with the identical curvature caused the angle at which the rays entered the LLGI to become higher than the acceptance angle for the liquid light guide. The angle that the rays entered at was measured by using a polar iso-candela plot (Figure 3). With further optimization it should be feasible to achieve illumination by 16 LEDs using this configuration.

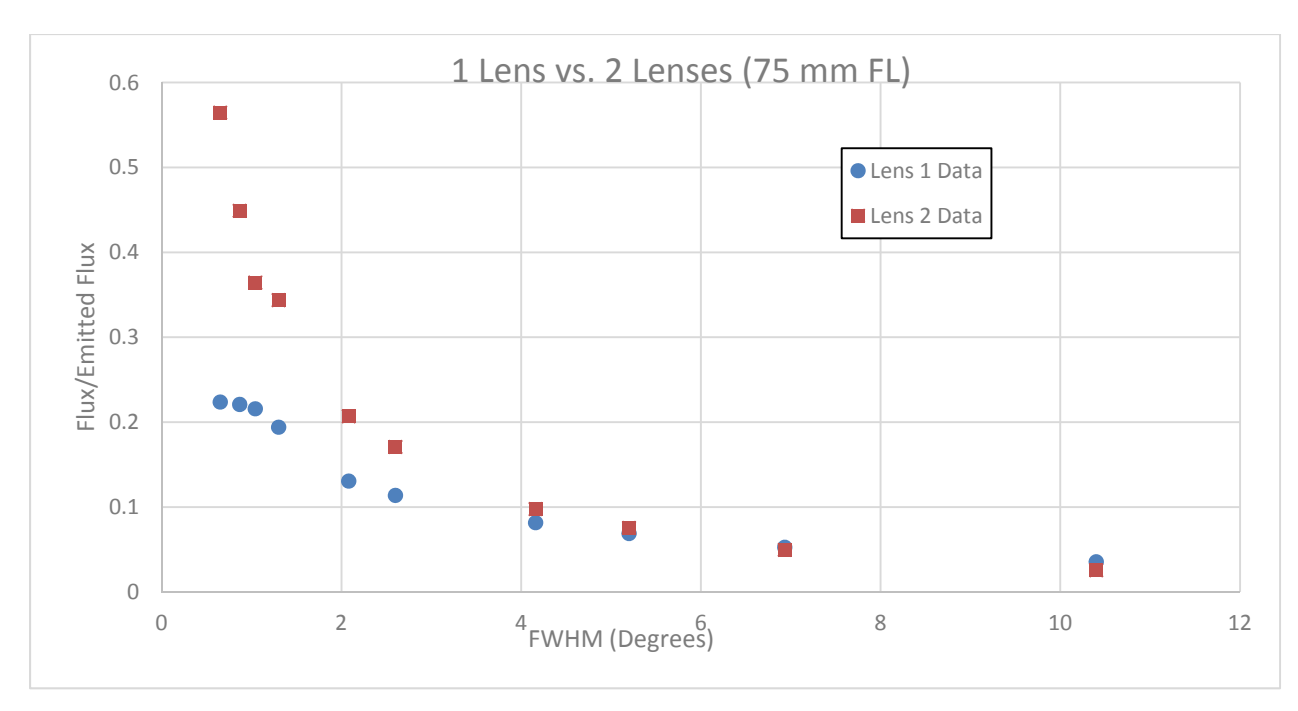


Figure 5 – Graph of the transmission vs full-width half-maximum (FWHM) of LED viewing angle data for the single and dual lens configuration using a 75 mm FL lens in a 152.4-mm FL mirror configuration. To achieve a narrowed viewing angle, the irradiance angular profile was divided by an integer value, such as 2, achieving a fraction of the original FWHM angular dispersion.

4.0 FUTURE WORK

Future work will focus on implementing the configuration starting with modeling and manufacturing the concave mirror. The configuration will need to have a mechano-optical structure designed to contain it and hold all of its parts. This will be done via 3D modeling with specific parts being printed in house and others being outsourced to be manufactured. Once the prototype is implemented the experimental performance will be evaluated.

5.0 ACKNOWLEDGEMENTS

The authors would like to acknowledge support from NIH Grants P01HL066299 and R01HL137030, NSF grant 1725937, and the Abraham Mitchell Cancer Research Fund. Drs. Leavesley and Rich disclose financial interest in a start-up company formed to commercialize spectral imaging technologies, SpectraCyte, LLC.

REFERENCES

- [1] Young, M.R., "Principles and Technique of Fluorescence Microscopy," Journal of Cell Science s3-102(60), 419–449 (1961).
- [2] Lakowicz, J.R., and Masters, B.R., "Principles of Fluorescence Spectroscopy, Third Edition," Journal of Biomedical Optics 13(2), 029901 (2008).
- [3] Schultz, R.A., Nielsen, T., Zavaleta, J.R., Ruch, R., Wyatt, R., and Garner, H.R., "Hyperspectral imaging: A novel approach for microscopic analysis," Cytometry 43(4), 239–247 (2001).
- [4] Zimmermann, T., Rietdorf, J., and Pepperkok, R., "Spectral imaging and its applications in live cell microscopy," FEBS letters 546(1), 87–92 (2003).
- [5] Harris, A.T., "Spectral mapping tools from the earth sciences applied to spectral microscopy data," Cytometry Part A 69A(8), 872–879 (2006).
- [6] Leavesley, S.J., Annamdevula, N., Boni, J., Stocker, S., Grant, K., Troyanovsky, B., Rich, T.C., and Alvarez, D.F., "Hyperspectral imaging microscopy for identification and quantitative analysis of

- fluorescently-labeled cells in highly autofluorescent tissue," Journal of Biophotonics 5(1), 67–84 (2012).
- [7] Garini, Y., Young, I.T., and McNamara, G., "Spectral imaging: Principles and applications," Cytometry Part A 69A(8), 735–747 (2006).
- [8] Li, Q., He, X., Wang, Y., Liu, H., Xu, D., and Guo, F., "Review of spectral imaging technology in biomedical engineering: achievements and challenges," Journal of Biomedical Optics 18(10), 100901 (2013).
- [9] Lu, G., and Fei, B., "Medical hyperspectral imaging: a review," Journal of Biomedical Optics 19(1), 010901 (2014).
- [10] Favreau, P.F., Hernandez, C., Heaster, T., Alvarez, D.F., Rich, T.C., Prabhat, P., and Leavesley, S.J., "Excitation-scanning hyperspectral imaging microscope," Journal of Biomedical Optics 19(4), 046010 (2014).
- [11] Annamdevula, N.S., Sweat, B., Favreau, P., Lindsey, A.S., Alvarez, D.F., Rich, T.C., and Leavesley, S.J., "An Approach for Characterizing and Comparing Hyperspectral Microscopy Systems," Sensors 13(7), 9267–9293 (2013).
- [12] Leavesley, S.J., Sweat, B., Abbott, C., Favreau, P., and Rich, T.C., "A theoretical-experimental methodology for assessing the sensitivity of biomedical spectral imaging platforms, assays, and analysis methods," Journal of Biophotonics 11(1), e201600227 (2018).
- [13] Browning, C.M., Mayes, S., Rich, T.C., and Leavesley, S.J., "Design of a modified endoscope illuminator for spectral imaging of colorectal tissues," in Opt. Biopsy XV Real-Time Spectrosc. Imaging Diagn. 10060, 1006015 (2017).
- [14] Mayes, S.A., Moore, K., Browning, C., Klomkaew, P., Rich, T.C., and Leavesley, S.J., "Applications and assessment of an excitation-scanning hyperspectral imaging system," in Imaging Manip. Anal. Biomol. Cells Tissues XVI 10497, 1049706 (2018).
- [15] Leavesley, S.J., Walters, M., Lopez, C., Baker, T., Favreau, P.F., Rich, T.C., Rider, P.F., and Boudreaux, C.W., "Hyperspectral imaging fluorescence excitation scanning for colon cancer detection," Journal of Biomedical Optics 21(10), 104003 (2016).
- [16] Deal, J., Mayes, S., Browning, C., Hill, S., Rider, P., Boudreaux, C., Rich, T., and Leavesley, S.J., "Identifying molecular contributors to autofluorescence of neoplastic and normal colon sections using excitation-scanning hyperspectral imaging," Journal of Biomedical Optics 24(2), 021207 (2018).